

1 A multimodal imaging approach enables *in vivo* assessment of antifungal treatment in
2 a mouse model of invasive pulmonary aspergillosis

3 Jennifer Poelmans,^{a,c} Uwe Himmelreich,^{a,c} Liesbeth Vanherp,^{a,c} Luca Zhai,^{a,c} Amy
4 Hillen,^{a,c*} Bryan Holvoet,^{b,co} Sarah Belderbos,^{a,c} Matthias Brock,^d Johan Maertens,^e
5 Greetje Vande Velde,^{a,c#} Katrien Lagrou,^f

6 ^aBiomedical MRI unit, Department of Imaging and Pathology, KU Leuven, Leuven,
7 Belgium;

8 ^bNuclear Medicine and Molecular Imaging, Department of Imaging and Pathology, KU
9 Leuven, Leuven, Belgium.

10 ^cMoSAIC, Department of Imaging and Pathology, KU Leuven, Leuven, Belgium.

11 ^dFungal Biology Group - School of Life Sciences, University of Nottingham,
12 Nottingham, United Kingdom.

13 ^eHematology, Department of Immunology and biology, KU Leuven, Leuven, Belgium.

14 ^fLaboratory of Clinical Bacteriology and Mycology, Department of Microbiology and
15 Immunology, KU Leuven, Leuven, Belgium.

16 Running Title: Multimodal imaging of IPA treatment in a mouse model

17 #Address correspondence to prof. Greetje Vande Velde,
18 greetje.vandavelde@kuleuven.be

19 *Present address: Amy Hillen, Department of Cell and Molecular Biology (CMB),
20 Karolinska Institutet, Stockholm, Sweden.

21 ^oPresent address: Bryan Holvoet, Terumo Europe, Leuven, Belgium.

22 G.V.V. and K.L. contributed equally to this work.

23 **Abstract**

24 *Aspergillus fumigatus* causes life-threatening lung infections in immunocompromised
25 patients. Mouse models are extensively used in research to assess the *in vivo* efficacy
26 of antifungals. In recent years, there has been an increasing interest in the use of non-
27 invasive imaging techniques to evaluate experimental infections. However, single
28 imaging modalities have limitations concerning the type of information they can
29 provide. In this study, magnetic resonance imaging and bioluminescence imaging were
30 combined to obtain longitudinal information on the extent of developing lesions and
31 fungal load in a leucopenic mouse model of IPA. This multimodal imaging approach
32 was used to assess changes occurring within lungs of infected mice receiving
33 voriconazole treatment starting at different time points after infection. Results showed
34 that IPA development depends on the inoculum size used to infect animals and that
35 disease can be successfully prevented or treated by initiating intervention during early
36 stages of infection. Furthermore, we demonstrated that reduction of the fungal load is
37 not necessarily associated with the disappearance of lesions on anatomical lung
38 images, especially when antifungal treatment coincides with immune recovery. In
39 conclusion, multimodal imaging allows to investigate different aspects of disease
40 progression or recovery by providing complementary information on dynamic
41 processes, which are highly useful for assessing the efficacy of (novel) therapeutic
42 compounds in a time- and labor-efficient manner.

43 **Introduction**

44 *Aspergillus fumigatus* is an opportunistic pathogen which is ubiquitous in the
45 environment (1). Inhalation of fungal spores can result in invasive pulmonary
46 aspergillosis (IPA), especially in patients with prolonged neutropenia or underlying
47 hematopoietic malignancies (2-5). Voriconazole and isavuconazole are recommended
48 first line treatment options for invasive aspergillosis (6, 7). In addition to antifungal
49 treatment, reversal of the underlying immunosuppression is also a key element in the
50 successful management of IPA (7).

51 Preclinical research plays an important role in investigating the pathogenesis of IPA
52 and in testing antifungal treatment strategies. In a previous study, we showed that
53 anatomical imaging techniques such as magnetic resonance imaging (MRI) and
54 computed tomography (CT) are highly suitable to monitor dynamic disease-related
55 changes in a leucopenic mouse model of IPA (8). The non-invasive character of these
56 techniques did not only allow for the longitudinal visualization of developing lung
57 lesions, but also for the quantification of imaging-derived biomarkers such as the lung
58 tissue volume. However, besides obtaining insight into structural changes occurring in
59 the lung upon infection, it is also crucial to obtain information on fungal growth in order
60 to fully comprehend all aspects of developing disease and treatment response. As an
61 alternative for standard invasive techniques such as colony-forming unit (CFU)
62 counting to assess infection, there has been great interest in using non-invasive
63 imaging techniques to quantify the fungal load.

64 Bioluminescence imaging (BLI) is an optical technique based on the detection of
65 photons, which are generated by an enzymatic reaction upon luciferin substrate
66 administration (9). To apply this imaging modality in the infectious diseases field,
67 pathogens have to be genetically modified to express the luciferase enzyme. As only

68 viable cells can produce bioluminescent signals, the detected signal can be used to
69 determine dynamic changes in the microbial load of an organ. Therefore, the obtained
70 read-outs are comparable to results obtained by conventional CFU counting (10). BLI
71 has already been used extensively to study bacterial and viral infections in both
72 superficially located organs such as the skin and deeply located organs such as the
73 lungs (11-19). Unfortunately, transforming fungi to express luciferase turned out to be
74 more challenging. Initial studies focused on the transformation of *Saccharomyces*
75 *cerevisiae* and *Candida albicans* (20, 21). *In vivo*, only partial success was obtained
76 with the bioluminescent *C. albicans* strain using *Renilla* or surface-anchored *Gaussia*
77 luciferase (22-25). It proved to be feasible to monitor superficial infections, but
78 limitations in the availability of the substrate coelenterazine and absorption of the
79 emitted light (480 nm) by hemoglobin hampered the detection of deep-seated
80 infections. These difficulties were overcome by using a codon-optimized firefly
81 luciferase, which enabled to study disseminated candidiasis and revealed an
82 unexpected persistence of *C. albicans* in the gall bladder under antifungal therapy (26).

83 The firefly luciferase has also been successfully used to monitor invasive aspergillosis
84 caused by *A. fumigatus* (10). In a first approach of using the bioluminescent strain, it
85 was possible to visualize the early stages of disease in a cortisone-induced mouse
86 model of IPA. However, imaging of late stage disease was hampered by restrictions in
87 oxygen and substrate availability at the lesion site due to the strong inflammatory
88 response and associated necrosis. Further studies revealed that the choice of immune
89 suppressive regimen has an important impact on the evolution of bioluminescence
90 during progression of disease (27). In contrast to the cortisone model, disease
91 progression in cyclophosphamide-induced mice was associated with a strong increase
92 in BLI signal over time due to rapid fungal growth and lung tissue invasion.

93 Furthermore, it was shown that animals treated with lipid amphotericin or voriconazole
94 show a transient increase in BLI signal, followed by a clear decrease in case of
95 treatment success (28). These results highlight the added value of using BLI for
96 obtaining information on changes in fungal burden occurring within the lungs of
97 leucopenic mice suffering from IPA.

98 In most studies, single imaging techniques are used to assess disease progression
99 and treatment response, which strongly limits the amount and type of acquired
100 information (8, 10, 28). In this study, both an optical and anatomical imaging technique
101 were combined to non-invasively obtain complementary information on IPA
102 development in a leucopenic mouse model. Furthermore, the influence of voriconazole
103 treatment on both the fungal load and lesion size was longitudinally investigated. The
104 aim of this study was to improve our knowledge on the relationship between detected
105 lesion and fungal growth in a completely non-invasive manner.

106 **Materials and Methods**

107 **Fungal strain**

108 The bioluminescent *Aspergillus fumigatus* strain 2/7/1 was used (28). The strain was
109 cultured for 3 days at 42°C on diluted Sabouraud agar, containing 10% of the dextrose
110 and peptone concentrations used in regular Sabouraud agar. Conidia were harvested
111 by flooding the agar with saline-0.1% Tween 80 (Sigma-Aldrich, Diegem, Belgium) and
112 gently scraping the surface. The collected suspension was shaken vigorously for 5
113 minutes and spores were counted with a Neubauer haemocytometer. The suspension
114 was diluted to a final concentration of 2.5×10^7 spores/ml or 1.0×10^7 spores/ml.

115 **Mouse model**

116 All animal experiments were carried out in compliance with national and European
117 regulations and were approved by the animal ethics committee of KU Leuven. Ten-
118 week old male BALB/c mice (Janvier, Le Genest, France) were rendered leucopenic
119 by intraperitoneal (IP) injections of 150 mg/kg cyclophosphamide (Sigma-Aldrich,
120 Diegem, Belgium) on day 4 and 1 prior to infection. To confirm leucopenia, blood was
121 collected from a subset of animals by cardiac puncture and 3.8% trisodium citrate
122 dihydrate was added to the sample to prevent coagulation. White blood cells were
123 counted on day 0 (n = 3) and day 4 (n = 3) using the Advia 2120i hematology system
124 (Siemens Healthcare GmbH, Erlangen, Germany).

125 On day 0, the animals were anesthetized with 1.5-2% isoflurane (Abbott Laboratories,
126 Queenborough, UK) in 100% oxygen and intranasally instilled with 20 μ l of a
127 suspension containing either 5×10^5 (high inoculum) or 2×10^5 (low inoculum) *A.*
128 *fumigatus* spores, as previously described (8). Directly after instillation, the mice were
129 positioned upright until normal breathing was resumed. In this manuscript, all times are
130 stated relative to the day of inoculation, which will be referred to as day 0.

131 All animals in the treatment groups received daily IP injections of 20 mg/kg
132 voriconazole (Vfend®, Pfizer, New York, USA) dissolved in saline. For the high
133 inoculum group, treatment was initiated either on the day of infection (day 0; n = 5) or
134 on day 1 (n = 5), day 2 (n = 5) or day 3 (n = 5) post infection (PI). Based on the data
135 obtained for this high inoculum group, treatment was initiated directly on the day of
136 infection (day 0; n = 5) or on day 2 PI (n = 5) for the low inoculum group. To prevent
137 rapid metabolization of voriconazole, the drinking water was replaced by 100% grape
138 fruit juice (Carrefour brand, Boulogne Billancourt, France) as described before (29).
139 The disease course was monitored by acquiring MRI scans before infection (baseline)
140 and on day 1, 2, 3, 4, 5 and 14 PI. In addition, *in vivo* BLI scans were acquired on day
141 3, 5 and 9 PI. Non-treated animals (n = 10 for the high inoculum group; n = 5 for the
142 low inoculum group) did not receive voriconazole nor grape fruit juice. For these mice,
143 daily MRI and *in vivo* BLI scans were acquired until day 4 PI for the high inoculum
144 group and until day 7 PI for the low inoculum group.

145 During image acquisition, the mice were anesthetized with 1.5-2% isoflurane in 100%
146 O₂ administered via a nasal cone. Body weight, posture and body temperature were
147 monitored daily. The animals were sacrificed when humane endpoints were reached,
148 including a strong loss in body weight (> 25%), lethargy and labored breathing. For all
149 treatment groups, the remaining animals that did not reach the humane endpoints were
150 euthanized after the last imaging time point. After sacrificing, *ex vivo* BLI scans of the
151 isolated lungs were acquired.

152 **Bioluminescence Imaging**

153 Images were acquired using an IVIS Spectrum system (Perkin Elmer). For *in vivo*
154 imaging, anesthetized animals were placed in the flow chamber and D-luciferin was
155 injected subcutaneously (126 mg/kg). Next, images were acquired until the peak signal

156 intensity was reached. For *ex vivo* imaging, the complete lungs were inflated with 500
157 μ l D-luciferin (7.5 mg) by inserting a catheter (22-gauge) into the trachea, after which
158 the tissue was isolated and immediately placed in the flow chamber to perform a scan.
159 The BLI images were processed using the Living Image software (version 4.5.4, Perkin
160 Elmer, Hopkinton, USA). A circular region of interest (ROI) covering the complete lung
161 area was used to measure the total photon flux.

162 **Magnetic Resonance Imaging**

163 Images were acquired on a 9.4 Tesla Biospec small animal MRI scanner (20 cm
164 horizontal bore size; Bruker BioSpin, Ettlingen, Germany) using a gradient insert
165 (maximal field strength of 1200 mT/m) and a 3.5 cm quadrature resonator. Body
166 temperature and breathing rate were continuously monitored and kept at physiological
167 values during the scans by using a physiological monitoring system (SAII, Stony Brook,
168 NY, USA). A 3D prospectively respiratory gated ultrashort echo time (UTE) pulse
169 sequence was used with following parameters: 0.03 ms echo time (TE), 15 ms
170 repetition time (TR), 5° flip angle (FA), 3.5 cm isotropic field of view (FOV), 128 x 128
171 x 128 matrix, 273 μ m isotropic resolution and a total acquisition time of 18 minutes (8).

172 The acquired MR images were analyzed using an in-house written Mevislab module
173 (version 2.6.1; Mevislab Medical Solutions and Fraunhofer MEVIS, Bremen,
174 Germany). The lung tissue volume was quantified based on a volume of interest (VOI)
175 covering the complete lung by manually delineating a ROI on each image slice,
176 excluding the heart and main pulmonary vessels. Based on the receiver gain value of
177 individual scan, a variable threshold was used to select all voxels with a signal intensity
178 above this threshold. Furthermore, a cumulative image score was determined to semi-
179 quantitatively describe lesion development and progression by applying a previously
180 described scoring system (8).

181 **Fungal load quantification**

182 After the last imaging time point, all animals were euthanized by an overdose of
183 pentobarbital (Nembutal, CEVA Santé Animale, Diegem, Belgium). After performing
184 *ex vivo* BLI, the right lung lobes were removed for fungal load quantification by colony-
185 forming unit (CFU) counting. The lungs were weighed and homogenized in 600 μ l
186 phosphate-buffered saline (PBS). Fivefold dilution series were prepared and plated on
187 Sabouraud agar, followed by three days incubation at 30°C and manual counting of
188 CFUs (30).

189 **Histological analysis**

190 The left lung lobe was isolated, post-fixed (24 hours in 10%-formalin) and embedded
191 in paraffin. The entire lung was sectioned (5 μ m) and stained with periodic acid-Schiff
192 (PAS), staining fungi in red (31).

193 **Statistics**

194 The data were analyzed using Prism (version 5.04; GraphPad software, San Diego,
195 CA). Repeated measures ANOVA with a Tukey's post-test was used to investigate
196 changes in total photon flux (BLI), lung tissue volume and cumulative image score
197 (MRI) over time in the non-treated high inoculum group. Linear regression analysis was
198 performed to assess the correlation between BLI and MRI derived biomarkers.
199 Student's t-test was used to evaluate differences in total photon flux (*ex vivo* BLI) and
200 CFU counts between the treated and non-treated groups. Differences were considered
201 statistically significant if p-value < 0.05. In all figures, the data is represented as mean
202 \pm standard deviation (SD).

203

204 **Results**

205 **Longitudinal assessment of fungal load and lung anatomy changes by** 206 **combining MRI and BLI**

207 In this study, mice were rendered leucopenic by two injections of cyclophosphamide.
208 All circulating white blood cells were depleted at the time of infection, meaning there
209 were 37.0 ± 6.4 neutrophils, 96.3 ± 33.9 lymphocytes, 0 ± 0 monocytes, 3.7 ± 6.4
210 eosinophils and 0 ± 0 basophils / μl present in the blood. In leucopenic mice, pulmonary
211 infection is characterized by excessive hyphal growth (32). In order to mimic clinic
212 management where reversal of immunosuppression is needed for clearance of the
213 fungal infection, no additional boosters of cyclophosphamide post infection were
214 administered. Consequently, the immune system recovered by day 4, which was
215 reflected by a mean neutrophil count of 162.9 ± 23.12 cells / μl blood.

216 Visual assessment of the MR images revealed the presence of hyper intense lesions
217 within the infected lungs on day 3 and 4 post infection (figure 1A). Both the lung tissue
218 volume and cumulative image score quantified from these MR images increased over
219 time, reaching significance on day 3 and 4 compared to baseline (figures 1B-C). Upon
220 visual inspection of the corresponding bioluminescence images, high signal intensities
221 emerged from the lung area on day 3 and 4 after instillation (figure 1D). Furthermore,
222 a bioluminescent signal appeared in the nose region starting from day 2. The total
223 photon flux quantified from the lung region increased over time, becoming significant
224 from day 2 onwards (figure 1E). After comparing BLI and MRI derived parameters, a
225 strong positive correlation was identified between the total photon flux and the lung
226 tissue volume ($R^2 = 0.65$) and between the total photon flux and cumulative image
227 score ($R^2 = 0.76$) (figure 2A-B). By performing *in vivo* BLI, longitudinal information was

228 obtained on the amount of viable fungal cells present in the lesions detected on the
229 anatomical MR images of infected mouse lungs.

230 **Non-invasive detection of changes in lesion composition resulting from** 231 **antifungal treatment**

232 The combination of both imaging modalities could also be used to obtain a better
233 understanding of the effect of antifungal treatment on the development and
234 composition of lung lesions. To assess differences in therapy response, voriconazole
235 treatment was initiated on the day of infection (day 0) or on day 1, 2, 3 after infection
236 with a high inoculum. The general condition of the animals was monitored daily and
237 anatomical lung MR images were acquired on day 1-5 and 14. None of the animals
238 receiving treatment starting at day 3 survived longer than 4 days post infection (figure
239 3A). The MR lung images of these animals showed detectable lesions starting from
240 day 3 (figure 3C-D, light grey bars). Initiating treatment earlier after infection strongly
241 improved the survival rates, as 60% of animals treated from day 2 survived until day
242 14 (figure 3A). However, the MRI scans revealed a gradual increase of lung lesions
243 over time in all animals, proving that treatment did not prevent disease progression in
244 this group (figure 3B-D; second row - medium grey bars). Animals receiving treatment
245 from day 1 post infection also displayed an improved survival rate (figure 3A). Unlike
246 the previous groups, most mice did not develop MR-detectable lesions within the lungs
247 (figure 3B, third row). Only two animals out of five showed clear lesion development
248 and needed to be sacrificed by day 4 or 5. As a result, both quantitative MRI-derived
249 biomarkers increased on day 4 and 5, followed by a strong decrease by day 14 (figure
250 3C-D, dark grey bars). When voriconazole treatment was started immediately after
251 infection, 80% of the animals survived until day 14 (figure 3A). Only a limited amount

252 of small lesions developed within the lungs of these animals (figure 3B-D; fourth row -
253 black bars).

254 The MRI results of the different treatment groups demonstrated a clear relationship
255 between the timing of treatment initiation and lesion development rate. To obtain
256 information on potential changes in the fungal load during treatment, *in vivo* BLI scans
257 were acquired on day 3, 5 and 9. Intense BLI signals were observed in the lung area
258 of animals receiving treatment starting from day 3 (figure 4A). All animals of this
259 treatment group needed to be sacrificed at the latest by day 4, explaining the lack of
260 data on later time points (figure 4B). Animals receiving treatment starting from day 2
261 also showed clear BLI signal from the lung region on day 3 (figure 4C). This signal
262 seemed to decrease by day 5 and returned to background levels by day 9 (figure 4D).
263 The quantified values were an order of magnitude lower on day 3 compared to the
264 group with treatment starting at day 3. The majority of animals in which treatment was
265 initiated on day 1 did not show any bioluminescent signal on day 3, 5 and 9 (figure 4E-
266 F). However, the two animals showing lesions on the lung MR images also displayed
267 clear BLI signal originating from the lung region on day 3. As these animals had to be
268 sacrificed by day 5, no BLI data was available on later time points. None of the animals
269 receiving treatment from day 0 showed any detectable BLI signal from the lung area
270 (figure 4G-H). Both MRI and BLI results indicate that initiation of treatment during the
271 early stages of infection has a beneficial effect on both the survival and disease state
272 of the animal.

273 **Improved treatment success in animals infected with a low inoculum of spores**

274 Therapy might affect disease progression differently when animals are infected with a
275 low number of fungal spores, as this model is associated with a high inter-animal
276 variation in infection development (8). To further assess this hypothesis, leucopenic

277 mice were instilled with 2×10^5 spores and voriconazole treatment was initiated on day
278 0 or day 2. The animals were followed-up by *in vivo* MRI (day 1-5 and 14) and *in vivo*
279 BLI scans (day 3, 5, 9). A separate control group did not receive treatment and was
280 scanned daily until day 7. Half of the non-treated mice needed to be sacrificed by day
281 4, while the remaining animals survived until day 7. Lesions could be visualized within
282 the lungs of 80 % of the non-treated mice and quantified as an increase in lung tissue
283 volume and cumulative image score over time (figure 5A-C). Furthermore, BLI signal
284 was detected from the lung region of the majority of animals by day 4, associated by a
285 decrease in BLI signal in the surviving mice (figure 5D-F). Within the lungs of mice
286 receiving treatment from day 2, small lesions could be detected on the MR images
287 from day 4 onwards (figure 5A-C; second row). However, no BLI signal could be
288 detected from the lung region of any animal from this group (figure 5E-F). Animals
289 receiving treatment from day 0 did not develop any detectable lesions within the lungs
290 (figure 5A-C, F). These results show an improved therapeutic response in animals
291 infected with a low inoculum, even if treatment is initiated at later time points post
292 infection.

293 ***Ex vivo* analysis of the lungs support the *in vivo* imaging findings**

294 After the last *in vivo* imaging time point, animals were euthanized and the lungs were
295 isolated to perform *ex vivo* BLI, CFU counting and histology. The lungs of non-treated
296 mice infected with a high inoculum showed a strong BLI signal, which was associated
297 with high total photon flux values and a high amount of counted colonies (figure 6A-C,
298 light grey). Comparable CFU counting results were obtained for the animals where
299 treatment commenced on day 3 (figure 6C). On the contrary, no BLI signal could be
300 detected from the lungs of mice receiving treatment from day 0 or 1 and no colonies
301 could be grown from their lung tissue (figure 6A-C, black and dark grey). Animals

302 receiving treatment from day 2 displayed modest BLI signals in the lungs and
303 significantly lower amounts of colonies could be grown from the tissue compared to
304 the non-treated group (figure 6A-C, medium grey). For animals infected with a low
305 inoculum, the lack of treatment (control group) resulted in a strong BLI signal,
306 originating from the lungs (figure 7A-B, light grey). Furthermore, colonies could be
307 grown from the lung tissue of most of the animals (figure 7C). In contrast, no clear BLI
308 signal could be detected nor could any colony be grown from the lungs for both
309 treatment groups (figure 7A-C, black and medium grey).

310 Histological analysis revealed the presence of large amounts of fungal elements within
311 the lungs of non-treated animals infected with a high inoculum (figure 8A). Fungal
312 hyphae invaded the airways and blood vessels, thereby destroying the bronchial lining
313 and normal lung structure. Comparable results were obtained for the animals receiving
314 treatment from day 3 onwards (data not shown). In contrast, no fungi were detectable
315 within the lungs of animals receiving treatment during early stages of infection (figure
316 8B). Massive lung lesions were observed in the lungs of animals treated from day 2,
317 which mainly consisted of immune cells and only a limited number of fungal elements
318 (figure 8C). Infection with a low inoculum of fungal spores resulted in the development
319 of lesions in the majority of non-treated animals, which contained large amounts of
320 fungal elements (figure 8D). On the contrary, animals receiving treatment from day 0
321 and day 2 did not show clear lesions on histological lung sections (figure 8 E-F). In
322 conclusion, the *ex vivo* analysis of the lungs confirmed the *in vivo* multimodal imaging
323 results.

324 **Discussion**

325 This study revealed the potential of combining multimodal imaging approaches to study
326 fungal disease development and treatment success. The acquired MR images
327 revealed the development of extensive lesions within the lung, which is in line with our
328 previously published results (8). In parallel, a strong increase in bioluminescence
329 signal intensity was observed from the lung area during the course of disease. These
330 observations indicate that the lung lesions detected by MRI are predominantly
331 composed of viable fungal cells. Furthermore, a strong bioluminescence signal
332 originating from the nose area likely resulted from fungal colonization or infection of
333 the nasopharynx or sinuses (28). Switching from an intranasal to an intratracheal
334 model could potentially avoid this secondary infection. Multimodal imaging allowed us
335 to non-invasively obtain dynamic information on both fungal load and lesion size in a
336 leucopenic IPA mouse model, which is of interest when assessing the effect of
337 antifungals.

338 We also investigated the feasibility to non-invasively monitor the effects of voriconazole
339 treatment, including reductions of the fungal load and potential changes in lesion
340 formation. Voriconazole was therefore administered at different time points after fungal
341 spore instillation. Starting treatment at the latest stage of infection proved to be
342 inefficient in counteracting disease progression. This is conform to the clinical situation,
343 in which late start of treatment is associated to a poor survival rate (6). On the contrary,
344 initiating treatment during the very first stages of infection successfully prevented IPA
345 development. The survival rates improved drastically and no pathological changes
346 could be detected within the lungs. These results support the clinical concept that early
347 diagnosis and treatment administration are essential to successfully recover from IPA
348 and underlines the importance of preemptive antifungal treatment in high-risk patient

349 populations. Furthermore, we showed that the treatment efficacy was higher in animals
350 infected with a low inoculum, even when treatment was initiated as late as 48 hours
351 after instillation. The fungal burden is generally lower in these mice, which facilitates
352 controlling the infection by administration of antifungal compound in combination with
353 the restoring immune system.

354 Most preclinical studies initiate treatment immediately after inducing infection, because
355 it increases the success rate for obtaining a positive response. However, studying the
356 delayed therapeutic effect of a compound is much more relevant, as it facilitates the
357 translation of preclinical results into a clinical setting. Previous studies showed that
358 non-invasive imaging techniques can only detect infection as early as 48 hours post
359 instillation in the cyclophosphamide mouse model (8, 28). Based on this information, a
360 true therapeutic treatment strategy was assessed in our imaging study by initiating
361 voriconazole administration on day 2 post infection. The majority of animals survived
362 for the total observation period of two weeks, which is indicative for treatment success.
363 However, MR imaging revealed the clear development of lung lesions, which kept on
364 increasing in size over time. The associated BL images showed a transient increase
365 in lung signal, meaning that the lesions detected by MRI still contained a high amount
366 of viable fungal cells up to 24 hours after the first administration of voriconazole. At
367 later time points, the number of viable fungi decreased drastically, although lesions did
368 not resolve on the MR images. Histopathological analysis of those lesions revealed a
369 massive influx of immune cells at the lesion sites. All animals were rendered leucopenic
370 at the time of infection, but no additional boosters of cyclophosphamide were
371 administered. This resulted in recovery of the immune system by day 4 and enabled
372 the development of the observed inflammatory response⁽³³⁾. Altogether, these findings
373 demonstrate that the improvements observed in animals treated from day 2 resulted

374 from an interplay between the fungicidal effect of voriconazole and the inflammatory
375 processes initiated upon reversal of leucopenia. This slows down lesion growth and
376 leads to a change in lesion composition rather than the disappearance of induced
377 lesions.

378 In clinical practice, decisions concerning discontinuation of antifungal treatment in IPA
379 patients are based on several factors, including immune status and evidence of
380 resolution of clinical signs and symptoms of disease (6, 7). In general, the improvement
381 of lesions detected by CT is considered as strong evidence of treatment success.
382 However, multiple clinical studies revealed that a worsening of pulmonary lesions is
383 not necessarily associated with progressing IPA (34-36). Antifungal treatment is,
384 whenever possible, combined with a reduction of immunosuppressive therapy to
385 improve patient outcome, but neutrophil recovery can potentially result in the
386 development of a pulmonary immune reconstitution inflammatory syndrome (IRIS).
387 This syndrome causes a massive influx of immune cells at the site of infection, leading
388 to an increase in lesion size and thus a worsening of radiological findings (34, 35). Both
389 IRIS and refractory IPA are associated with an increase in lesion volume on CT
390 images, making it difficult to distinguish between these two different conditions
391 although both require different treatment approaches. There is a need to gather more
392 information on IRIS in the context of IPA management and its impact on disease
393 recovery. Preclinical research could play a role in assessing new treatment and
394 management options, as it was shown in our study that a potential development of IRIS
395 can non-invasively be identified in a leucopenic IPA mouse model by the combined
396 use of BLI and MRI. However, further in depth studies are needed to confirm the
397 development of IRIS and may require a larger number of animals and the use of
398 additional markers. This can then be combined by the proposed multimodal imaging

399 approach to longitudinally assess the impact of adapting the treatment regimen on the
400 lesion composition and outcome of the subject.

401 In conclusion, we showed that the combination of BLI and MRI is highly suitable to
402 evaluate different aspects of progressing IPA in leucopenic mice, as it provides
403 complementary information on dynamic changes in fungal load as well as lung lesion
404 development. Furthermore, we were able to gain insights in therapy-induced changes
405 concerning both the extent and the composition of lesions, which is crucial to fully
406 comprehend different aspects of disease recovery or deterioration. We believe that
407 multimodal imaging will become increasingly important in future preclinical studies as
408 a tool to evaluate the *in vivo* efficacy of therapeutic compounds in a time-efficient
409 manner.

410 **Acknowledgements**

411 This work was supported by funding provided by the Flemish research foundation
412 (FWO; G.0691.15N and 1506114N) and KU Leuven IF and BOF (CREA/14/015,
413 STG/15/024, C24/17/061). JP and BH received a PhD grant for strategic basic
414 research from the Agency for Innovation by Science and Technology (IWT). LV is a SB
415 PhD fellow at FWO. The work of MB was supported by the Transregio 124 FungiNet
416 project A3 from the German Science Foundation (DFG). GVV received a postdoctoral
417 fellowship from the FWO. Use of the bioluminescent *Aspergillus fumigatus* 2/7/1 strain
418 was granted by the Leibniz Institute for Natural Product Research and Infection Biology
419 (Hans Knöll Institute, Jena, Germany). All preclinical imaging was performed at the
420 Molecular Small Animal Imaging Centre of KU Leuven.

421 **References**

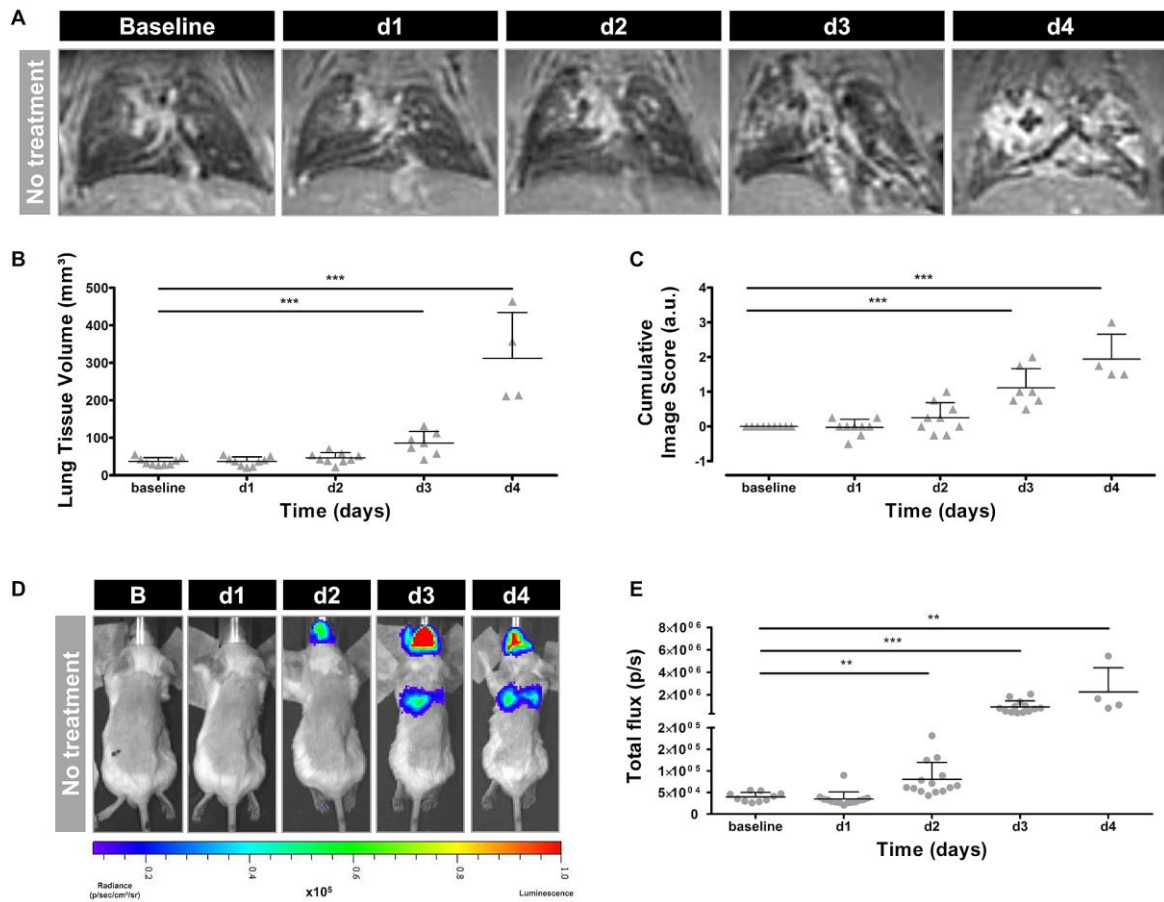
- 422 1. Pasqualotto AC. 2010. *Aspergillosis : from diagnosis to prevention*, 1st ed. Springer,
423 Dordrecht.
- 424 2. Pagano L, Caira M, Candoni A, Offidani M, Martino B, Specchia G, Pastore D, Stanzani
425 M, Cattaneo C, Fanci R, Caramatti C, Rossini F, Luppi M, Potenza L, Ferrara F, Mitra
426 ME, Fadda RM, Invernizzi R, Aloisi T, Picardi M, Bonini A, Vacca A, Chierichini A,
427 Melillo L, de Waure C, Fianchi L, Riva M, Leone G, Aversa F, Nosari A. 2010. Invasive
428 aspergillosis in patients with acute myeloid leukemia: a SEIFEM-2008 registry study.
429 *Haematologica* 95:644-50.
- 430 3. Feldmesser M. 2006. Role of neutrophils in invasive aspergillosis. *Infect Immun*
431 74:6514-6.
- 432 4. Silveira F, Paterson DL. 2005. Pulmonary fungal infections. *Curr Opin Pulm Med*
433 11:242-6.
- 434 5. Smith JA, Kauffman CA. 2012. Pulmonary fungal infections. *Respirology* 17:913-26.
- 435 6. Walsh TJ, Anaissie EJ, Denning DW, Herbrecht R, Kontoyiannis DP, Marr KA,
436 Morrison VA, Segal BH, Steinbach WJ, Stevens DA, van Burik JA, Wingard JR,
437 Patterson TF. 2008. Treatment of aspergillosis: clinical practice guidelines of the
438 Infectious Diseases Society of America. *Clin Infect Dis* 46:327-60.
- 439 7. Patterson TF, Thompson GR, 3rd, Denning DW, Fishman JA, Hadley S, Herbrecht R,
440 Kontoyiannis DP, Marr KA, Morrison VA, Nguyen MH, Segal BH, Steinbach WJ,
441 Stevens DA, Walsh TJ, Wingard JR, Young JA, Bennett JE. 2016. Practice Guidelines
442 for the Diagnosis and Management of Aspergillosis: 2016 Update by the Infectious
443 Diseases Society of America. *Clin Infect Dis* 63:e1-e60.
- 444 8. Poelmans J, Hillen A, Vanherp L, Govaerts K, Maertens J, Dresselaers T, Himmelreich
445 U, Lagrou K, Vande Velde G. 2016. Longitudinal, *in vivo* assessment of invasive
446 pulmonary aspergillosis in mice by computed tomography and magnetic resonance
447 imaging. *Lab Invest* 96:692-704.
- 448 9. Gammon ST, Foje N, Brewer EM, Owers E, Downs CA, Budde MD, Leevy WM,
449 Helms MN. 2014. Preclinical anatomical, molecular, and functional imaging of the lung
450 with multiple modalities. *Am J Physiol Lung Cell Mol Physiol* 306:L897-914.
- 451 10. Brock M, Jouvion G, Droin-Bergere S, Dussurget O, Nicola MA, Ibrahim-Granet O.
452 2008. Bioluminescent *Aspergillus fumigatus*, a new tool for drug efficiency testing and
453 *in vivo* monitoring of invasive aspergillosis. *Appl Environ Microbiol* 74:7023-35.
- 454 11. Demidova TN, Gad F, Zahra T, Francis KP, Hamblin MR. 2005. Monitoring
455 photodynamic therapy of localized infections by bioluminescence imaging of
456 genetically engineered bacteria. *J Photochem Photobiol B* 81:15-25.
- 457 12. Lu Z, Dai T, Huang L, Kurup DB, Tegos GP, Jahnke A, Wharton T, Hamblin MR. 2010.
458 Photodynamic therapy with a cationic functionalized fullerene rescues mice from fatal
459 wound infections. *Nanomedicine (Lond)* 5:1525-33.
- 460 13. Engelsman AF, van Dam GM, van der Mei HC, Busscher HJ, Ploeg RJ. 2010. *In vivo*
461 evaluation of bacterial infection involving morphologically different surgical meshes.
462 *Ann Surg* 251:133-7.
- 463 14. Francis KP, Yu J, Bellinger-Kawahara C, Joh D, Hawkinson MJ, Xiao G, Purchio TF,
464 Caparon MG, Lipsitch M, Contag PR. 2001. Visualizing pneumococcal infections in
465 the lungs of live mice using bioluminescent *Streptococcus pneumoniae* transformed
466 with a novel gram-positive lux transposon. *Infect Immun* 69:3350-8.
- 467 15. Smith MW, Schmidt JE, Rehg JE, Orihuela CJ, McCullers JA. 2007. Induction of pro-
468 and anti-inflammatory molecules in a mouse model of pneumococcal pneumonia after
469 influenza. *Comp Med* 57:82-9.

- 470 16. Hertlein T, Sturm V, Jakob P, Ohlsen K. 2013. 19F magnetic resonance imaging of
471 perfluorocarbons for the evaluation of response to antibiotic therapy in a *Staphylococcus*
472 *aureus* infection model. PLoS One 8:e64440.
- 473 17. Luker KE, Hutchens M, Schultz T, Pekosz A, Luker GD. 2005. Bioluminescence
474 imaging of vaccinia virus: effects of interferon on viral replication and spread. Virology
475 341:284-300.
- 476 18. Luker GD, Prior JL, Song J, Pica CM, Leib DA. 2003. Bioluminescence imaging reveals
477 systemic dissemination of herpes simplex virus type 1 in the absence of interferon
478 receptors. J Virol 77:11082-93.
- 479 19. Cook SH, Griffin DE. 2003. Luciferase imaging of a neurotropic viral infection in intact
480 animals. J Virol 77:5333-8.
- 481 20. Vieites JM, Navarro-Garcia F, Perez-Diaz R, Pla J, Nombela C. 1994. Expression and
482 in vivo determination of firefly luciferase as gene reporter in *Saccharomyces cerevisiae*.
483 Yeast 10:1321-7.
- 484 21. McNabb DS, Reed R, Marciniak RA. 2005. Dual luciferase assay system for rapid
485 assessment of gene expression in *Saccharomyces cerevisiae*. Eukaryot Cell 4:1539-49.
- 486 22. Srikantha T, Chandrasekhar A, Soll DR. 1995. Functional analysis of the promoter of
487 the phase-specific WH11 gene of *Candida albicans*. Mol Cell Biol 15:1797-805.
- 488 23. Srikantha T, Klapach A, Lorenz WW, Tsai LK, Laughlin LA, Gorman JA, Soll DR.
489 1996. The sea pansy *Renilla reniformis* luciferase serves as a sensitive bioluminescent
490 reporter for differential gene expression in *Candida albicans*. J Bacteriol 178:121-9.
- 491 24. Nakayama H, Mio T, Nagahashi S, Kokado M, Arisawa M, Aoki Y. 2000. Tetracycline-
492 regulatable system to tightly control gene expression in the pathogenic fungus *Candida*
493 *albicans*. Infect Immun 68:6712-9.
- 494 25. Enjalbert B, Rachini A, Vedyappan G, Pietrella D, Spaccapelo R, Vecchiarelli A,
495 Brown AJ, d'Enfert C. 2009. A multifunctional, synthetic *Gaussia princeps* luciferase
496 reporter for live imaging of *Candida albicans* infections. Infect Immun 77:4847-58.
- 497 26. Jacobsen ID, Luttich A, Kurzai O, Hube B, Brock M. 2014. In vivo imaging of
498 disseminated murine *Candida albicans* infection reveals unexpected host sites of fungal
499 persistence during antifungal therapy. J Antimicrob Chemother 69:2785-96.
- 500 27. Ibrahim-Granet O, Jouvion G, Hohl TM, Droin-Bergere S, Philippart F, Kim OY, Adib-
501 Conquy M, Schwendener R, Cavaillon JM, Brock M. 2010. In vivo bioluminescence
502 imaging and histopathologic analysis reveal distinct roles for resident and
503 recruited immune effector cells in defense against invasive aspergillosis. BMC
504 Microbiol 10:105.
- 505 28. Galiger C, Brock M, Jouvion G, Savers A, Parlato M, Ibrahim-Granet O. 2013.
506 Assessment of efficacy of antifungals against *Aspergillus fumigatus*: value of real-time
507 bioluminescence imaging. Antimicrob Agents Chemother 57:3046-59.
- 508 29. Sugar AM, Liu XP. 2000. Effect of grapefruit juice on serum voriconazole
509 concentrations in the mouse. Med Mycol 38:209-12.
- 510 30. Gupta VK, Tuohy MG. 2013. Laboratory protocols in fungal biology: Current methods
511 in fungal biology. Springer New York, New York.
- 512 31. Roden AC, Schuetz AN. 2017. Histopathology of fungal diseases of the lung. Semin
513 Diagn Pathol 34:530-549.
- 514 32. Dagenais TR, Keller NP. 2009. Pathogenesis of *Aspergillus fumigatus* in Invasive
515 Aspergillosis. Clin Microbiol Rev 22:447-65.
- 516 33. Huyan XH, Lin YP, Gao T, Chen RY, Fan YM. 2011. Immunosuppressive effect of
517 cyclophosphamide on white blood cells and lymphocyte subpopulations from peripheral
518 blood of Balb/c mice. Int Immunopharmacol 11:1293-7.

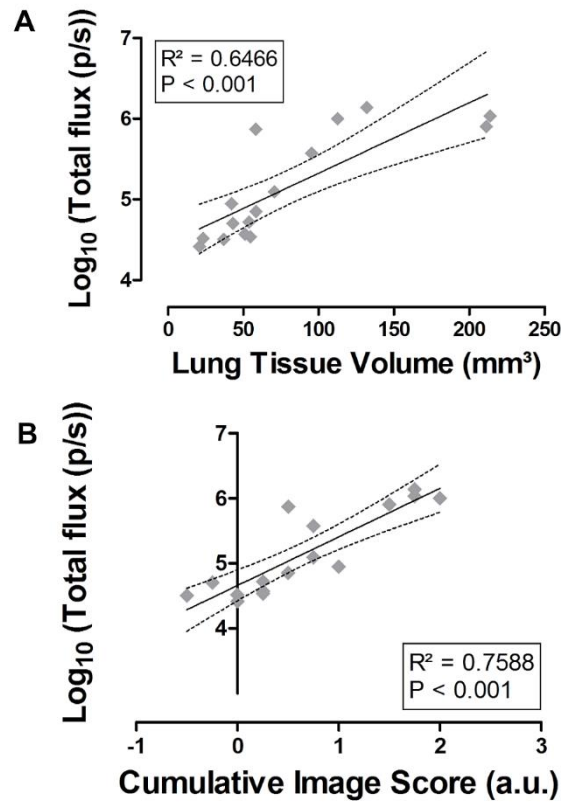
- 519 34. Miceli MH, Maertens J, Buve K, Graziutti M, Woods G, Rahman M, Barlogie B,
520 Anaissie EJ. 2007. Immune reconstitution inflammatory syndrome in cancer patients
521 with pulmonary aspergillosis recovering from neutropenia: Proof of principle,
522 description, and clinical and research implications. *Cancer* 110:112-20.
- 523 35. Jung J, Hong HL, Lee SO, Choi SH, Kim YS, Woo JH, Kim SH. 2015. Immune
524 reconstitution inflammatory syndrome in neutropenic patients with invasive pulmonary
525 aspergillosis. *J Infect* 70:659-67.
- 526 36. Caillot D, Couaillier JF, Bernard A, Casasnovas O, Denning DW, Mannone L, Lopez J,
527 Couillault G, Piard F, Vagner O, Guy H. 2001. Increasing volume and changing
528 characteristics of invasive pulmonary aspergillosis on sequential thoracic computed
529 tomography scans in patients with neutropenia. *J Clin Oncol* 19:253-9.

530

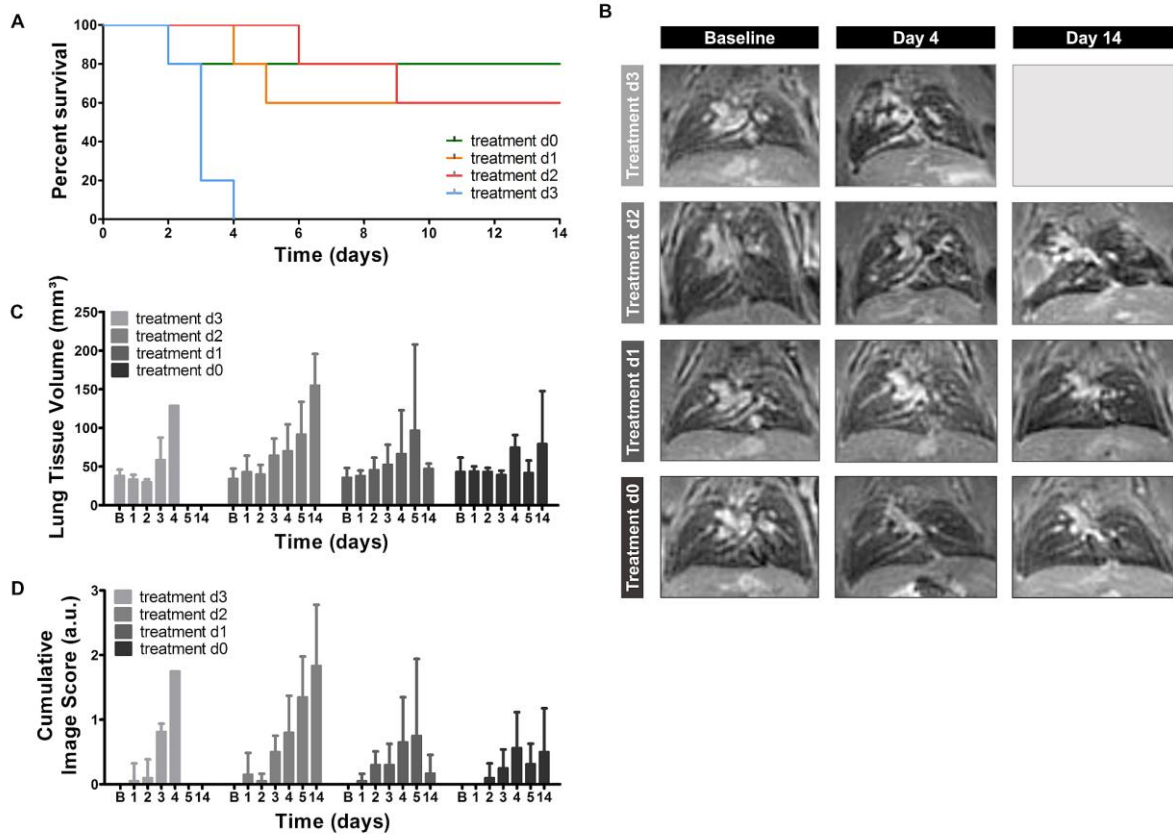
Figures & figure legends



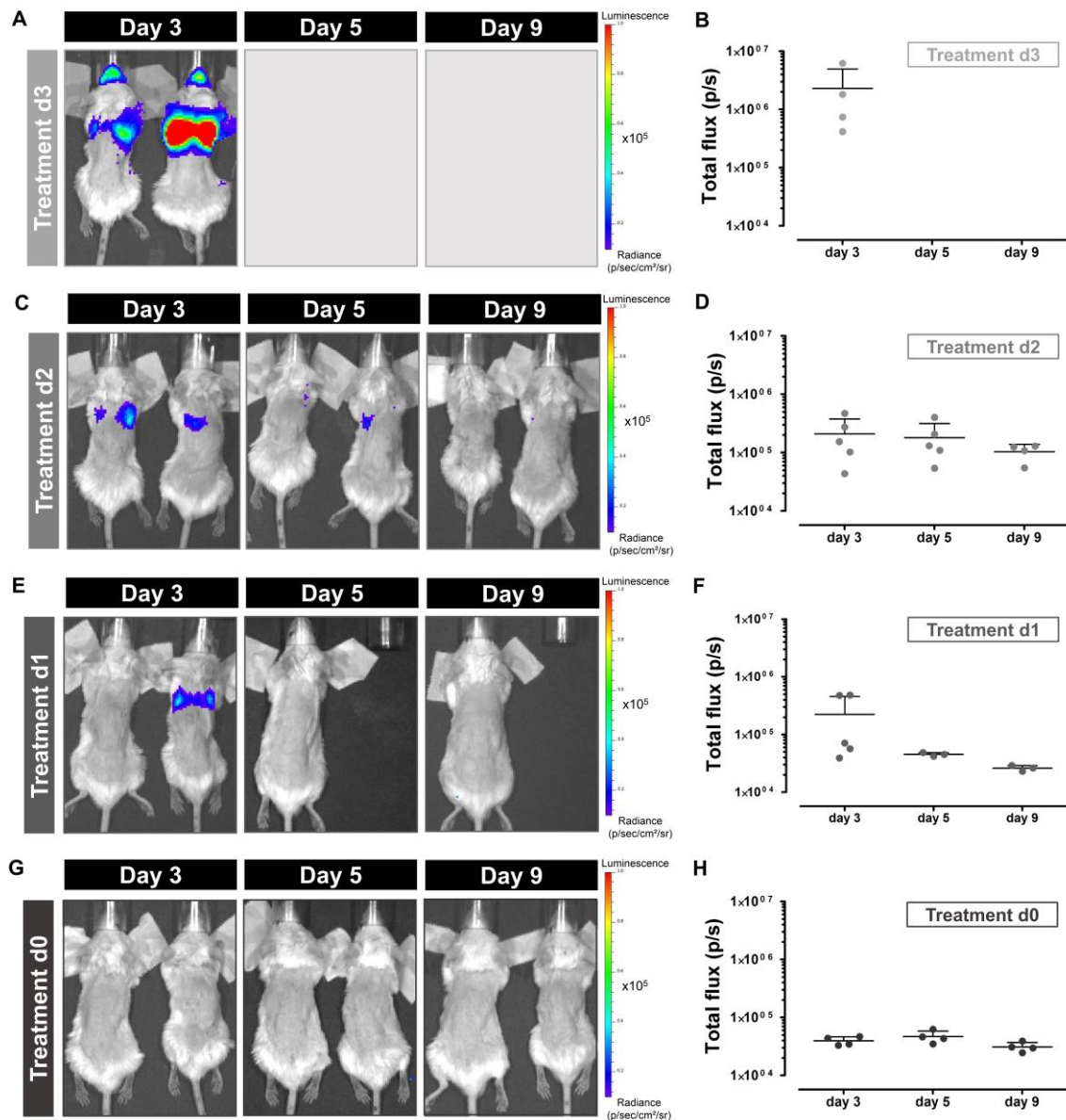
1 **Figure 1: Multimodal imaging of non-treated mice infected with a high inoculum**
 2 **of *A. fumigatus* spores.** (A) Representative 3D-UTE MR images of the lung before
 3 (Baseline) and after infection. (B-C) Graphs representing the lung tissue volume and
 4 cumulative image score quantified from the 3D-UTE MR images. (D) Representative
 5 BL images acquired before (Baseline) and after infection. (E) Graph representing the
 6 total photon flux quantified from the BLI images based on a circular ROI covering the
 7 complete lung region. Error bars represent SD of multiple mice (n = 10). *: p < 0.05; **: p < 0.01; ***: p < 0.001.



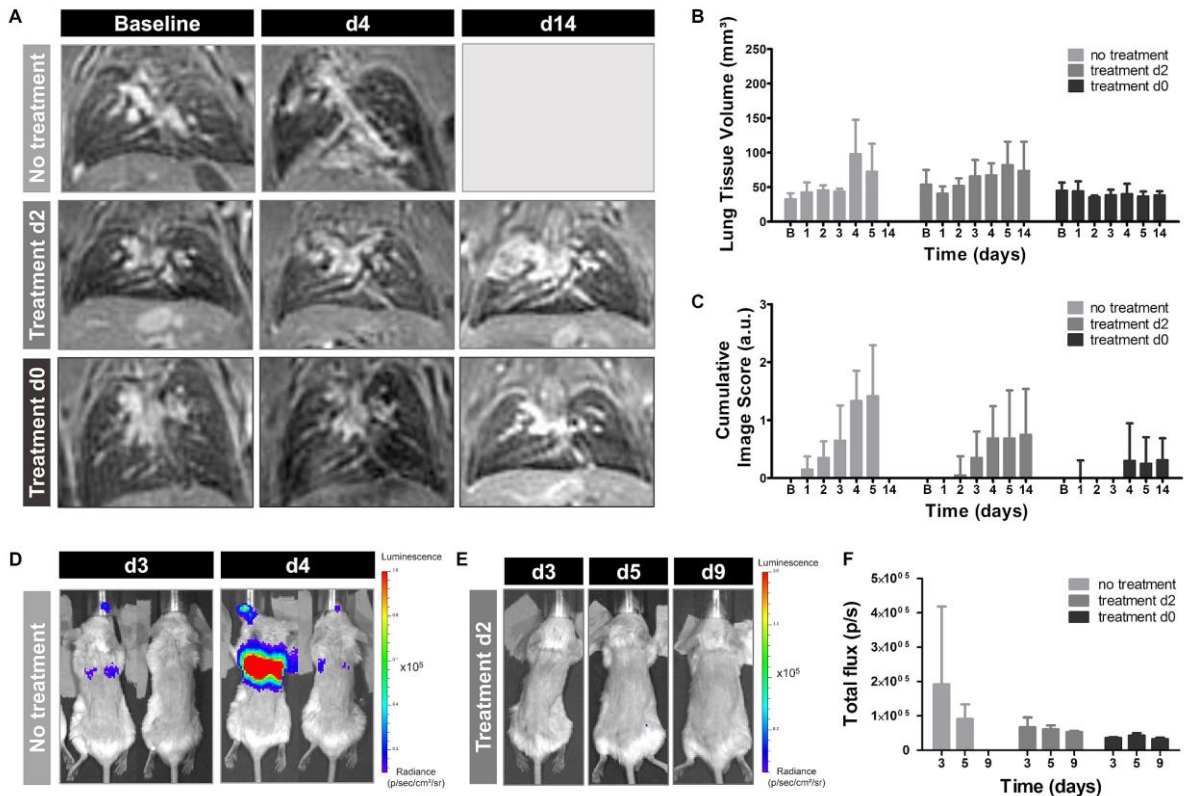
9 **Figure 2: Agreement between parameters quantified from BLI and MRI.** (A) Linear
 10 regression analysis of the BLI-derived total photon flux versus the MRI-derived lung
 11 tissue volume. (B) Linear regression analysis of the BLI-derived total photon flux versus
 12 the MRI-derived cumulative image score, expressed in arbitrary units. Dashed lines
 13 represent the 95% confidence band.



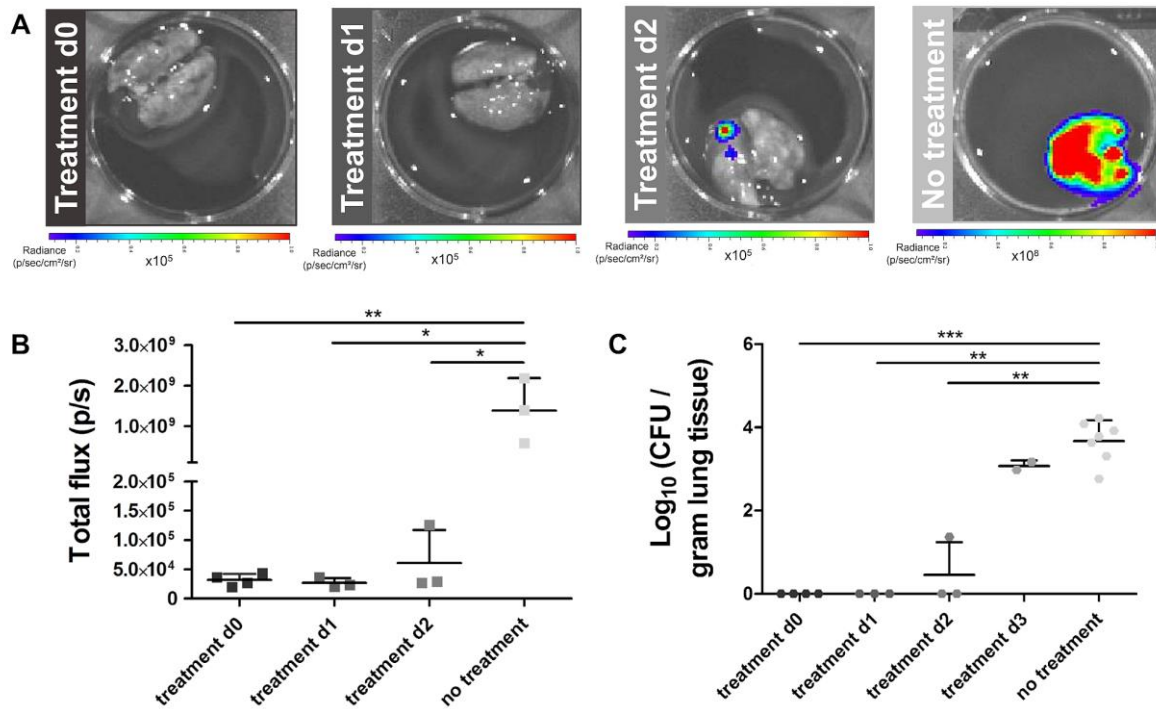
14 **Figure 3: MR imaging of animals infected with a high inoculum of *A. fumigatus***
 15 **spores receiving voriconazole at different time points.** (A) Survival curve including
 16 all treatment groups. (B) Representative 3D-UTE MR images of the lung before
 17 (Baseline) and after infection of all treatment groups. (C-D) Graphs representing the
 18 lung tissue volume and cumulative image score quantified from the 3D-UTE MR
 19 images for all treatment groups. Error bars represent SD of multiple mice (n = 5 per
 20 treatment group). *: p < 0.05; **: p < 0.01; ***: p < 0.001.



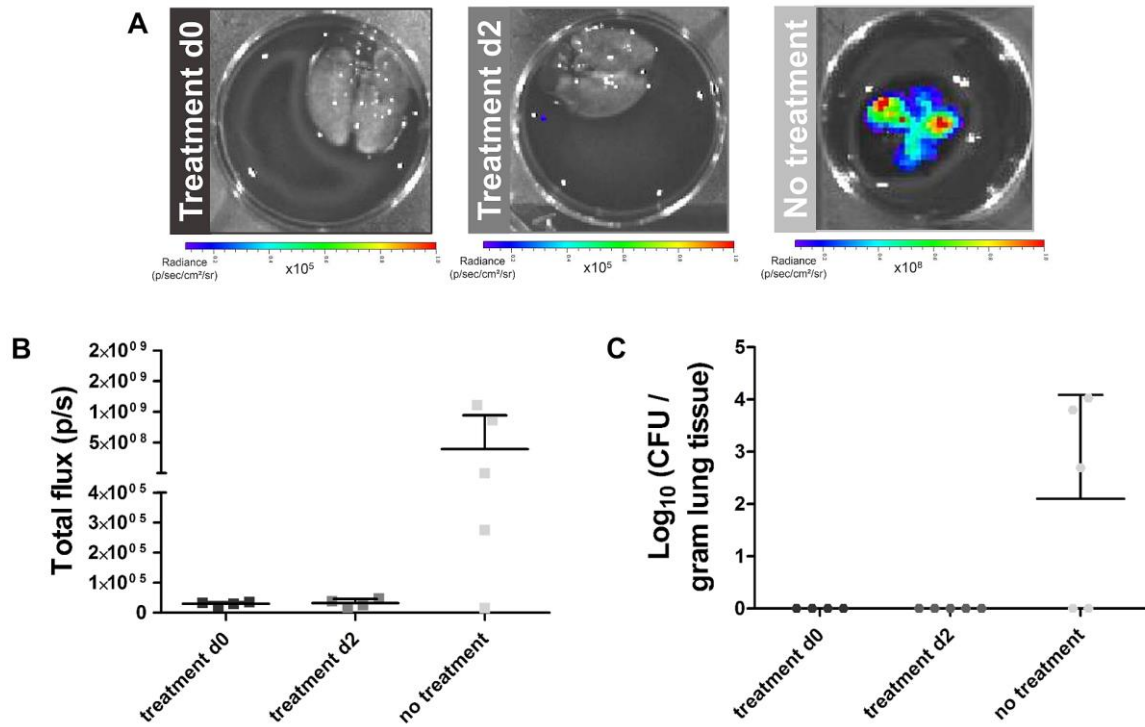
21 **Figure 4: Bioluminescence imaging of animals infected with a high inoculum of**
 22 ***A. fumigatus* spores receiving voriconazole from different time points.**
 23 Representative BLI images and associated graphs showing the total photon flux of
 24 infected mice receiving treatment from day 3 (A-B), day 2 (C-D), day 1 (E-F) or
 25 immediately after infection (G-H). Error bars represent SD of multiple mice (n = 5 per
 26 treatment group).



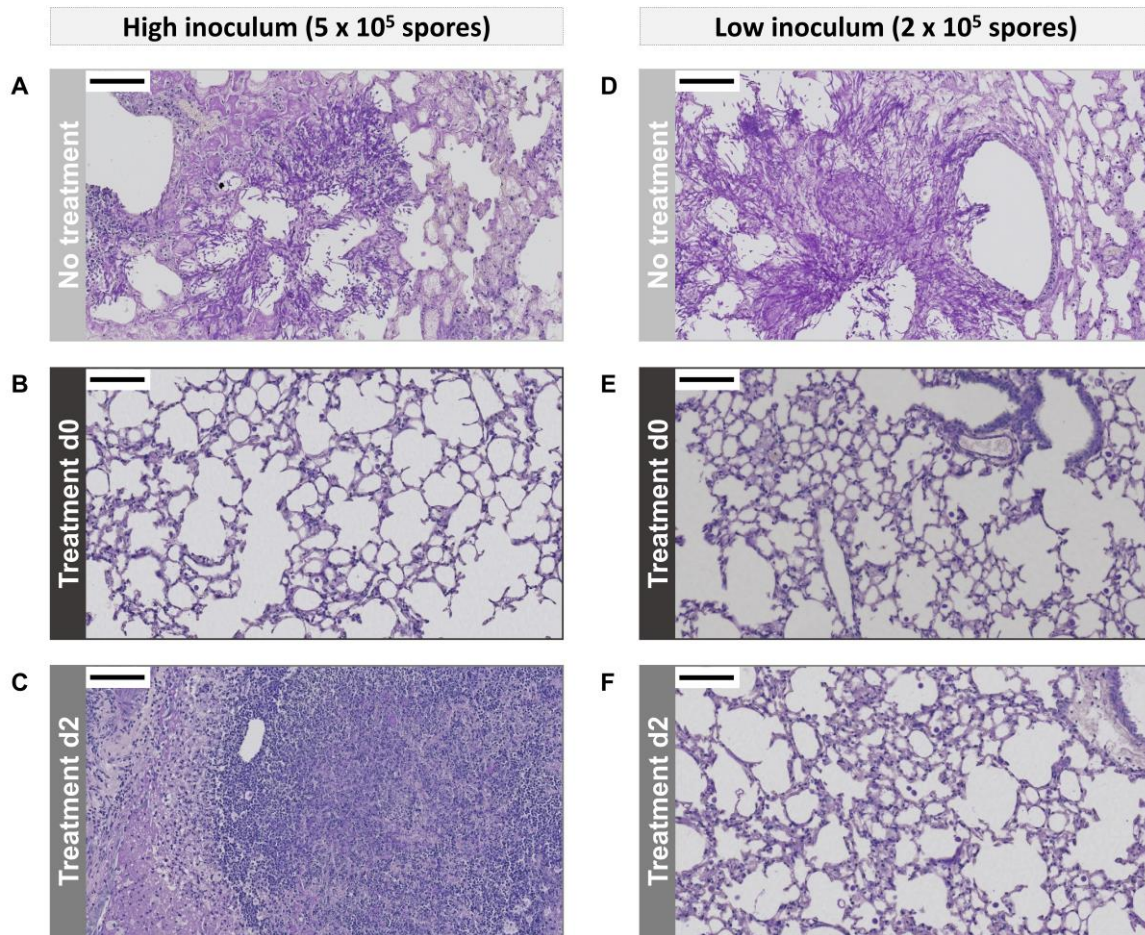
27 **Figure 5: Multimodal imaging of mice infected with a low inoculum of *A.***
 28 ***fumigatus* spores.** (A) Representative 3D-UTE lung MR images of non-treated
 29 animals and animals receiving voriconazole from day 2 or immediately after infection.
 30 (B-C) Graphs representing the lung tissue volume and cumulative image score
 31 quantified from the 3D-UTE MR images for all animal groups. (D) Representative BLI
 32 images of non-treated animals on day 3 and 4 after infection. (E) Representative BLI
 33 images of animals receiving treatment from day 2 on day 3, 5 and 9 after infection. (F)
 34 Graphs representing the total photon flux quantified from the BLI images for all animal
 35 groups. Error bars represent SD of multiple mice (n = 5 per animal group).



36 **Figure 6: Ex vivo quantification of the fungal load for treated and non-treated**
 37 **animals infected with a high inoculum.** (A) Representative *ex vivo* BLI images of
 38 lungs isolated after the last imaging time point. (B) Graph representing the total photon
 39 flux quantified from the *ex vivo* BLI images using a circular ROI covering the lungs. (C)
 40 Graph representing the amount of counted colonies per gram of lung tissue. Error bars
 41 represent SD. *: $p < 0.05$; **: $p < 0.01$; ***: $p < 0.001$.



42 **Figure 7: Ex vivo quantification of the fungal load for treated and non-treated**
 43 **animals infected with a low inoculum.** (A) Representative *ex vivo* BLI images of
 44 lungs isolated after the last imaging time point. B) Graph representing the total photon
 45 flux quantified from the *ex vivo* BL images using a circular ROI covering the lungs. (C)
 46 Graph representing the amount of counted colonies per gram of lung tissue. Error bars
 47 represent SD.



48 **Figure 8: Light microscopy images of PAS-stained lung sections.** Representative
 49 images of mice infected with a high inoculum of fungal spores without treatment (A) or
 50 after receiving treatment from day 0 (B) or day 2 (C). Representative images of mice
 51 infected with a low inoculum of fungal spores without treatment (D) or after receiving
 52 treatment from day 0 (E) or day 2 (F). The scale bars (upper left corner) measure 100
 53 μm . For both high and low inoculum groups, the lungs of non-treated animals were
 54 isolated on day 4 and the lungs of treated animals on day 14 post infection.